To appear in ApJ

Gamma-Ray Emission from the Broad-Line Radio Galaxy 3C 111

R. C. Hartman[1], M. Kadler[2,3,4], and J. Tueller[1]

Robert.C.Hartman@nasa.gov, matthias.kadler@sternwarte.uni-erlangen.de, Jack.Tueller@nasa.gov

ABSTRACT

The broad-line radio galaxy 3C 111 has been suggested as the counterpart of the γ–ray source 3EG J0416+3650. While 3C 111 meets most of the criteria for a high-probability identification, like a bright flat-spectrum radio core and a blazar-like broadband SED, in the Third EGRET Catalog, the large positional offset of about 1.5° put 3C 111 outside the 99% probability region for 3EG J0416+3650, making this association questionable. We present a re-analysis of all available data for 3C 111 from the EGRET archives, resulting in probable detection of high-energy γ–ray emission above 1000 MeV from a position close to the nominal position of 3C 111, in two separate viewing periods (VPs), at a 3σ level in each. A new source, GRO J0426+3747, appears to be present nearby, seen only in the >1000 MeV data. For >100 MeV, the data are in agreement with only one source (at the original catalog position) accounting for most of the EGRET-detected emission of 3EG J0416+3650. A follow-up *Swift* UVOT/XRT observation reveals one moderately bright X–ray source in the error box of 3EG J0416+3650, but because of the large EGRET position uncertainty, it is not certain that the X–ray and γ–ray sources are associated. A *Swift* observation of GRO J0426+3747 detected no X–ray source nearby.

Subject headings: gamma rays: observations — galaxies: active — galaxies: individual(3C 111)

[1]Astrophysics Science Division, NASA's Goddard Space Flight Center, Greenbelt, MD 20771, USA

[2]Dr. Karl Remeis-Observatory, University of Erlangen-Nuremberg, Sternwartstrasse 7, 96049 Bamberg, Germany

[3]CRESST/NASA Goddard Space Flight Center, Greenbelt, MD 20771, USA

[4]Universities Space Research Association, 10211 Wincopin Circle, Suite 500, Columbia, MD 21044, USA

1. Introduction

One of the main scientific goals of the recently-launched γ–ray astronomy satellite mission GLAST and its Large Area Telescope (LAT) (Ritz 2007; Michelson 2007) is to shed light on the nature of powerful relativistic extragalactic jets, which are ejected from the nuclei of some active galaxies (AGN). Originally, this class of AGN was defined based on the bright and prominent radio emission from these jets: the radio-loud population of active galaxies. Based on data from EGRET, the high-energy γ–ray telescope on the *Compton Gamma Ray Observatory*, it was realized (Fichtel 1994; Thompson et al. 1994; von Montigny et al. 1995) that the largest population of extragalactic γ–ray sources in the GeV regime is represented by those radio-loud AGN whose jets are pointed at a small angle to the line of sight. An intimate link is tied between radio VLBI and high-energy γ–ray astronomy by the fact that the bright compact radio emission of these so-called blazars provides excellent targets for parsec-scale resolution VLBI observations of their jet structure.

Of special interest are the questions of where in the AGN jets the bright γ–ray emission is produced, and how the emission is interacting with its immediate environment and with other parts of the jet. This knowledge would enable us to put crucial constraints on the processes of jet formation, collimation, and acceleration. GLAST is expected to yield densely sampled γ–ray light curves of hundreds of extragalactic jets that are bright enough to be detected on time scales of days to weeks, and thousands on time scales of months to years. Most of these objects will be blazars; in fact, all but two of the firmly identified extragalactic EGRET sources (LMC, Sreekumar et al. 1992; Centaurus A, Sreekumar et al. 1999) are blazars. In contrast to the blazars, most radio galaxies have larger inclination angles. That allows better (deprojected) linear resolution with VLBI observations, and in the case of stratified jet structures, it allows observations of the slower jet layers, e.g. a sheath, whose emission may be swamped by the much brighter beamed emission from faster jet regions, e.g. a fast spine, in blazars. Ghisellini et al. (2005) have presented such a spine-sheath stratified-jet model, predicting detectable γ–ray emission from the nuclei of some radio galaxies. In their model, each of the two emission regions sees photons coming from the other part relativistically enhanced because of the relative speed difference, giving rise to an additional inverse-Compton emission component.

In this letter we provide additional support for the identification of the broad-line radio galaxy 3C 111 as a γ–ray source, responsible for a portion of the source 3EG J0416+3650. Such an association was suggested as possible in the third EGRET catalog (Hartman et al. 1999, 3EG), but was considered unlikely because of the large positional offset of 3C 111 from 3EG J0416+3650. The present work was stimulated by the recent report of Sguera et al. (2005), who used multiwavelength data to strengthen the case for the association between

3C 111 and 3EG J0416+3650.

We show here that 3EG J0416+3650 is most likely composed of at least two, and more likely three, separate sources, one of which is in good positional agreement with 3C 111. As demonstrated recently, based on VLBA monitoring data at $\lambda 2$ cm from the MOJAVE program (Kadler et al. 2008), the parsec-scale jet of 3C 111 shows a variety of physically different regions in a relativistic extragalactic jet, such as a compact core, superluminal jet components, recollimation shocks, and regions of interaction between the jet and its surrounding medium, which are all possible sites of γ–ray production. Its relatively large inclination angle of $\sim$19° makes 3C 111 a particularly well-suited target for tests of structured-jet models, such as the model of Ghisellini et al. (2005). We describe our re-analysis of the available EGRET data on 3C 111, as well as follow-up *Swift* UVOT and XRT observation, in Sect. 2, and discuss our results and their implications in Sect. 3.

2. Analysis

2.1. EGRET Data Analysis

Using detailed analysis of reprocessed EGRET data[1], we have investigated the possibility that 3EG J0416+3650 is a superposition of at least two sources, one being at or near the position of 3C 111. The analysis for the 3EG catalog was based on photons with energies >100 MeV, for which the 68% containment angle of the spectrum-dependent point spread function (PSF) is always several degrees. For energies >1000 MeV, the half-angle of the cone containing 68 % of the photons from a source is considerably smaller, slightly less than one degree. On the other hand, the number of photons with energies above 1000 MeV is much smaller than that above 100 MeV. Both of those integral energy ranges were investigated for this study.

For each viewing period (VP) in which 3C 111 and 3EG J0416+3650 were in the EGRET field of view (FoV), the following procedure was initially used:

1. Using the standard EGRET likelihood software (LIKE), two sources were modeled, one at the 3EG position for 3EG J0416+3650 and one at the nominal position of 3C 111,

[1]The EGRET data reprocessing consisted of: 1) Manual examination of all events with energy >1000 MeV which had previously been rejected, adding a considerable number of events to the database; 2) adjustment of the EGRET sensitivity tables (Bertsch et al. 2001); 3) complete re-analysis of one viewing period (not used here) because of numerous errors in the original event selection.

and LIKE then provided the best estimates of the significance and flux of the two assumed sources.

2. If either of the two assumed sources had a test statistic (TS) of at least 4.0 (roughly 2σ), LIKE was then allowed to optimize the significance of the two sources by moving their positions.

The results from this procedure are shown in Table 1, for the two energy ranges and the two assumed sources. The first five columns show the VPs, the starting dates of the observations, the lengths of the VPs, and the off-axis angles of 3C 111. The line showing VP=P1234 is the analysis of the summed data for the VPs included in 3EG, VP0002 through VP4270. For each object and energy range, the table shows the maximum TS near the starting position, the change in position (from the starting point) to obtain the maximum TS, and the resulting photon flux in units of 10^{-8} photons $\mathrm{cm}^{-2}\,\mathrm{s}^{-1}$. Blank entries for TS indicate values of 0. For TS values less than 4.0, there are no entries in the next two columns. In addition to the VPs listed, VPs 0005, 0010, 0365, 2130, 2210, 4120, and 4260 were tested, and showed no indication (TS=0) of emission from either 3C 111 or 3EG J0416+3650; VP0390 also showed TS=0, but is shown in the table because it was the best exposure to the relevant sky region. For the cases where the offsets are small compared with the PSF, there is little difference in the TS and flux at the maximum TS positions compared with those at the original positions.

Considering that seven VPs are not shown because they yielded TS=0 for all four source/energy cases, the density of detections in this table is very low, even with the low requirement of TS$\geq$4.0. One of the 3C 111 detections (VP0150 for E>1000 MeV) has an offset position value larger than would be expected, and out of line with the other detections. It is discussed below.

Two VPs (0002 and 3211) provide reasonably strong detection of 3EG J0416+3650, which agrees with the information provided in 3EG. The summed exposure P1234 provides nearly the same significance of detection (but a much lower average flux than in VPs 0002 and 3211), indicating that the object was emitting γ rays at a low level even when it was not significantly detectable in individual VPs.

There are five results that support the proposed 3C 111 γ–ray source, two in E>100 MeV and three in E>1000 MeV. With the exception of VP0150 at >1000 MeV, the values of the position offsets are compatible with the position of 3C 111. Only one VP (0310) shows detections in both energy ranges. Like 3EG J0416+3650, 3C 111 appears to radiate γ rays with a low duty cycle, occasionally becoming fairly bright.

The number of photons >100 MeV from 3C 111 was 64, 44 of them in VP0310 and 14

in VP3215. Only about 20 photons >1000 MeV were detected from 3C 111, six in VP0150, four in VP0310, and four in VP3250.

For 3EG J0416+3650, there was a total of 152 photons >100 MeV, 37 of them in VP3211 (the most significant single detection) and 33 in VP0002. P1234 yielded seven photons above 1000 MeV from 3EG J0416+3650, but as indicated in Table 1, they produced a TS of only 3.1, about 1.8σ.

We have further investigated a small region around 3EG J0416+3650 by generating $5^\circ \times 5^\circ$ likelihood maps, for the energy ranges >100 MeV and >1000 MeV, for each VP in which 3C 111 and 3EG J0416+3650 were in the FoV. A sample of the more informative likelihood maps is shown in Figure 1. Maps for the summed data, P1234, are shown in Figure 2. The contours in the upper (>100 MeV) half of Figure 2 are similar to those in the corresponding figure from 3EG, but in the current version, the extension toward the 3C 111 position is more pronounced. We draw the following conclusions from these maps:

1. There appear to be at least three sources (possibly more) contributing, two in the >1000 MeV energy range and at least one in the >100 MeV range. One of the two >1000 MeV sources is very near the position of 3C 111; for the other, which is of comparable strength, we find no obvious identification (see below). In the following, we designate this source GRO J0426+3747; as seen from Figure 2, the 68 % confidence error on its position is about 0.8°.

2. Little or no significant emission is detected from the two >1000 MeV sources in the lower energy band.

3. The >100 MeV emission is dominated by a source near the 3EG catalog position. There is no significant detection in the >1000 MeV energy range. In the following, the name 3EG J0416+3650 refers implicitly to this source.

4. The >1000 MeV map for VP0150 shows why the position offset for 3C 111 is so large (0.43°) in Table 1 in that VP. There are only six photons that can be clearly attributed to 3C 111 in that map. One additional photon is nearly a degree away from 3C 111. This shifts the maximum likelihood position toward that single photon, which could be either from the tail of the PSF, or from the diffuse Galactic foreground.

As an additional check on the reality of the two >1000 MeV sources, we have compared the number of occurrences of $\geq 2\sigma$ excesses in 17 maps (5° by 5°) with the statistically expected value. The results are shown in Table 2. For the regions of the maps away from the two "source" positions, the number of $>2\sigma$ excesses is about as expected from statistical

fluctuations, taking into account the number of PSFs contained within each map. Near the locations of the two >1000 MeV sources, however, there are far more excesses than expected, which provides added confidence in the detections of 3C 111 and GRO J0426+3747. For each of VPs 0005 and 3215 (which had very low exposures), there was exactly one photon detected in the 5° x 5° region for which the TS maps were generated. Both of those photons were very close to the GRO J0426+3747 position obtained from the summed emission in P1234, well within the 68 % PSF extent. An examination of a somewhat larger region indicated that the probability of a photon from the diffuse emission that close to a particular point was less than 0.01. Those two events are indicated with "s" in Table 2.

2.2. *Swift* Follow-Up X-Ray Observations and Their Analysis

There are no known high-energy sources close to the nominal best-fit positions of 3EG J0416+3650 and GRO J0426+3747. Therefore, we have conducted follow-up optical/UV and X–ray observations with the UVOT and XRT instruments on the NASA satellite *Swift* (Gehrels et al. 2004). The 3EG J0416+3650 field was observed for 10.4 ksec on December 14, 2007[2], and the GRO J0426+3747 field for 9.0 ksec on 20 December, 2007[3]. No significant X–ray source was detected above the background level in the 23.6×23.6 arcsec XRT FoV around GRO J0416426+3747. The XRT observation of the 3EG J0416+3650 field detected one 4.8σ source at the position 04 h 15 m 54.3 s, +36 d 49 m 26 s, with an uncertainty of 5.8 arcsec.

We extracted spectra from the source (which we designate Swift J041554.3+364926) and background regions using XSELECT, and response and ancillary files provided by the *Swift* calibration data base (CALDB)[4]. The low count rate of 0.0026 ± 0.0006 cts $+s^{-1}$ limits the ability to derive spectral information. However, it is striking that only 4 photons (out of 26) were detected between 0.2 keV and 1 keV. To characterize the spectrum, we used Cash statistics (Cash 1979) in XSPEC and determined the maximum allowable power-law photon index in a power-law fit under the assumption of zero absorption, as may be expected from a very local source. The result is slightly dependent on the data binning chosen, but suggests a very hard spectrum, with the maximum allowed photon index in the range 1.1-1.3. If the absorption parameter is allowed to vary freely during the fit, the photon index is poorly constrained, and steeper values up to 2.7 are statistically allowed.

[2]Observation ID 00031057001

[3]Observation ID 00031072001

[4]`http://heasarc.gsfc.nasa.gov/docs/caldb/swift/`

2.3. Spectral energy distributions

The historical spectral energy distribution (SED) of 3C 111 is shown in Figure 3. The millimeter flux range was determined with permission from the SMA Submillimeter Calibrator List archived data[5] (Gurwell et al. 2007). The R-band flux range has been determined from data obtained in a long-term monitoring program with the Liverpool telescope (PI: I. McHardy) between November 2004 and July 2007 (S. Jorstad, priv. comm.).

The 3C 111 SED is similar to those of EGRET-detected flat-spectrum radio quasars (FSRQs), except that the rollover in the NIR, optical, and UV is steeper here. This makes the "valley" between the synchrotron and Compton "bumps" appear deeper. This could be due to absorption intrinsic to 3C 111, since the data points have been corrected for Galactic absorption.

Figure 4 shows (a) a UVOT image of the Swift J041554.3+364926 region, with a circle superimposed indicating the 1–σ position uncertainty for the X–ray source (as determined with the FTOOLS task XRTCENTROID); and (b) an SED containing the very limited multiwavelength data available for this source. The EGRET points shown are for comparison only; despite its proximity to the 3EG position for the γ–ray source, it is not certain that Swift J041554.3+364926 is actually the same object as 3EG J0416+3650, because the EGRET position uncertainty is quite large (about 0.63° in radius).

In the Swift J041554.3+364926 SED, the UVOT data are plotted twice, with and without dereddening, because it is not certain whether the object is nearby or extragalactic. The open circles denote the observed fluxes; the dereddened fluxes are shown as filled circles. Note that the fall-off in the optical-UV is extremely steep, especially in the observed fluxes. If Swift J041554.3+364926 is an extragalactic source, this can be attributed to absorption at the edge of a foreground molecular cloud, part of the Taurus complex, with absorbing column density $N_{\rm H} = 2.18 \times 10^{21}\,{\rm cm}^{-2}$ (Kalberla et al. 2005). NED shows A_V of 1.893 mag for the catalog position of the EGRET source, about 0.1° away. In the extragalactic scenario, Swift J041554.3+364926 must be a radio quiet source because of the very low upper limit on its radio flux density, 0.7 mJy at 1.4 GHz, from the NVSS survey (Condon et al. 1998). The shape of the dereddened UV/optical/IR range suggests an AGN "blue bump", usually attributed to thermal emission from an accretion disk. However, without far IR and/or submillimeter data points, it is not possible to be certain of this interpretation. Based on previous experience, a radio-quiet AGN is an unlikely identification for an EGRET source.

Alternatively, if Swift J041554.3+364926 is within our Galaxy, it would need to be an

[5] http://sma1.sma.hawaii.edu/callist/callist.html

M star or a cataclysmic variable (CV) in order to produce the observed X–rays (R. Osten and S. Drake, priv. comm.). In order to be visible optically, an M star would necessarily be in front of the molecular cloud, which is 140 pc distant (Elias 1978), so the observed UVOT data points should be considered, rather than the dereddened ones. The observed X–ray emission is stronger than expected from an M star except during an exceptional flare (R. Osten and S. Drake, priv. comm.). If the object is a CV, its luminosity is much greater, so it must be behind the Taurus absorber, making the dereddened UVOT points appropriate; in that case the X–ray emission is reasonable. Based on previous experience, neither an M star or a CV would be a likely identification for an EGRET source.

Table 3 and Table 4 provide the values plotted in Figures 3 and 4, with references.

3. Discussion and Conclusions

The γ–ray source 3EG J0416+3650 seems to be composed of at least three variable sources. One of the sources, detected only above 1000 MeV, is close to the radio galaxy 3C 111, and plausibly associated with it; a new source, GRO J0426+3747, is also seen only above 1000 MeV, and has no obvious identification at other wavelengths. Most of the flux >100 MeV is from the third source, for which there is no evidence in the >1000 MeV data. The position obtained here for the third source is very near the catalog position of 3EG J0416+3650. It might be associated with the XRT source Swift J041554.3+364926, but the EGRET position uncertainty makes a firm association impossible. The region under study is $8-10^\circ$ from the Galactic plane, so either 3EG J0416+3650 or GRO J0426+3747 (or both) could be local.

A recent stacking search found no evidence for γ–ray emmision from radio galaxies as a class (Cillis, Hartman, & Bertsch 2004). That paper specifically excluded 3C 111 from consideration because of its blazar-like superluminal motion, so there is no direct conflict with the results presented here. That study made no systematic cut on the angle to the line-of-sight of the radio jet, so for most of the galaxies included, that angle was considerably larger than the $\sim 19^\circ$ which has been estimated for 3C 111 (Kadler et al. 2008). Since a larger line-of-sight angle implies substantially smaller Doppler boosting and therefore lower γ–ray output, there is no obvious conflict between the present results and those of Cillis, Hartman, & Bertsch (2004). A more significant challenge is posed by the lack of EGRET detection of γ–ray emission from the (much closer) AGN M87. Superluminal motion has been detected in the jet knot HST-1, about 0.86 arcsec downstream from the radio core, both in the optical and radio bands (Biretta et al. 1999; Cheung et al. 2007). Most estimates of our line-of-sight angle to its jet are in the range $30-45^\circ$. If we assume that M87 is similar to 3C 111, it is

not clear whether its Doppler boosting is sufficiently low to compensate for its much smaller distance, and thereby account for its non-detection by EGRET.

Our re-analysis of the available EGRET data supports the previous association of 3EG J0416+3650 with the broad line radio galaxy 3C 111, but with 3C 111 responsible for only a portion of the γ–ray emission. Furthermore, it explains the relatively large positional offset noted in Hartman et al. (1999). We have compiled an historical SED of 3C 111 which shows that the X–ray data may well extrapolate into the EGRET range, particularly during flares, which is in agreement with the intermittent nature of detections in the individual EGRET viewing periods. It is interesting to note that we detect 3C 111 at almost exactly the γ–ray flux that is predicted by equation (12) in Ghisellini et al. (2005): $(1.41-14.1)\times10^{-11}\,\mathrm{erg\,s^{-1}\,cm^{-2}}$, scaling from the 5 GHz values in Table 3. Note that 3C 111 (z=0.0485) would be the most distant radio galaxy detected in γ rays, about twice as far as NGC 6251 (Mukherjee et al. 2002; z=0.0247).

The detection of γ–ray emission from 3C 111 further supports the hypothesis that radio galaxies may represent an important class of LAT sources. GLAST was launched on 11 June, 2008; its LAT detector will continuously scan the entire sky over a 3-hr interval. With a factor of 30 greater sensitivity than EGRET, and with a factor of $\sim$3 better PSF above 1 GeV, it will be more efficient than EGRET for detecting transients over the whole sky. In the case of 3C 111, GRO J0426+3747, and 3EG J0416+3650, the smaller PSF and greater effective area of the LAT will clearly separate these three sources.

We thank Goro Sato, Francesco Verrecchia, Svetlana Jorstad, and Chris Shrader for their help and advice in compiling the SED data for this study. Steve Drake and Rachel Osten have kindly provided insight regarding X–ray emission from stars. MK has been supported by the NASA Postdoctoral Program at the Goddard Space Flight Center, administered by Oak Ridge Associated Universities through a contract with NASA. This research has made use of data obtained from the High Energy Astrophysics Science Archive Research Center (HEASARC), provided by NASA's Goddard Space Flight Center, and the NASA/IPAC Extragalactic Database (NED), operated by the Jet Propulsion Laboratory, California Institute of Technology, under contract with NASA. We have also made use of data products from the Two Micron All Sky Survey, a joint project of the University of Massachusetts and the Infrared Processing and Analysis Center, California Institute of Technology, funded by NASA and NSF. Submillimeter flux ranges for 3C 111 were obtained from the on-line archives of the Submillimeter Array (SMA), a joint project between the Smithsonian Astrophysical Observatory and the Academia Sinica Institute of Astronomy and Astrophysics, funded by the Smithsonian Institution and the Academia Sinica.

REFERENCES

Beckmann, V., Gehrels, N., Shrader, C. R., & Soldi, S. 2006, ApJ, 638, 642

Bertch, D. L., Hartman, R. C., Hunter, S. D., Thompson, D. J., & Sreekumar, P. 2001, in AIP Conf. Proc. 587, Gamma 2001, ed. Ritz, S., Gehrels, N., & Shrader, C. R. (Melville, NY: AIP), 706

Biretta, J. A., Sparks, W. B., & Macchetto, F. 1999, ApJ, 520, 621

Cash, W. 1979, ApJ, 228, 939

Cillis, A. N., Hartman, R. C., & Bertsch, D. L. 2004, ApJ, 601, 142

Condon, J. J., Cotton, W. D., Greisen, E. W., Yin, Q. F., Perley, . A., Taylor, G. B., & Broderick, J. J. 1998, AJ, 115, 1693

Cheung, C. C., Harris, D. E., & Stawarz, Ł. 2007, ApJ, 663, L65

Dadina, M. 2007, A&A, 461, 1209

Elias, J. H. 1978, ApJ, 224, 857

Fichtel, C. E. 1994, ApJS, 90, 917

Gehrels, N., et al. 2004, ApJ, 611, 1005

Ghisellini, G., Tavecchio, F., & Chiaberge, M. 2005, A&A, 432, 401

Golombek, D., Miley, G. K., & Neugebauer, G. 1988, AJ, 95, 26

Gurwell, M. A., Peck, A. B., Hostler, S. R., Darrah, M. R., & Katz, C. A. 2007, From Z-Machines to ALMA: (Sub)Millimeter Spectroscopy of Galaxies, 375, 234

Hartman, R. C., et al. 1999, ApJS, 123, 79

Johnson, W. N., Zdziarski, A. A., Madejski, G. M., Paciesas, W. S., Steinle, H., & Lin, Y-C 1997, in AIP Conf. Proc. 410, Fourth Compton Symposium, ed. Dermer, C., Strickman, M., & Kurfess, J. (Woodbury, NY: AIP), 283

Kadler, M. 2005, PhD Thesis, University of Bonn, Bonn, Germany

Kadler, M., Ros. E., Perucho, M., et al. 2008, ApJ, 680, 867

Kalberla, P. M. W., Burton, W. B., Hartmann, D., Arnal, E. M., Bajaja, E., Morras, R., Pöppel, W. G. L. 2005, A&A, 440, 775

Lamb, R. C., and Macomb, D. J. 1997, ApJ, 488, 872

Maisack, M., Mannheim, K., & Collmar, W. 1997, A&A, 319, 397

Michelson, P. F. 2007, in AIP #921, "The First GLAST Symposium", Melville, New York, 8

von Montigny, C., et al. 1995 ApJ, 444, 525

Mukherjee, R., Halpern, J., Marabal, N., & Gotthelf, E. V. 2002, ApJ, 574, 693

Ritz, S. 2007, in AIP #921, "The First GLAST Symposium", Melville, New York, 3

Sguera, V., Bassani, L., Malizia, A., Dean, A. J., Landi, R., & Stephen, J. B. 2005, A&A, 430, 107

Sreekumar, P., et al. 1992, ApJ, 400, L67

Sreekumar, P., Bertsch, D. L., Hartman, R. C., Nolan, P. L., & Thompson, D. J. 1999, Astroparticle Physics, 11, 221

Skrutskie, M. F., et al. 2006, AJ, 131, 1163

Thompson, D. J., et al. 1994, in "Multi-Wavelength Continuum Emission of AGN", ed. Courvoisier, T. J.-L., & Bleha, A., (The Netherlands: IAU), 49

Tueller, J., Mushotzky, R. F., Barthelmy, S., Cannizzo, J. K., Gehrels, N., Markwardt, C. B., Skinner, G. K., & Winter, L. M. 2007, ArXiv e-prints, 711, arXiv:0711.4130

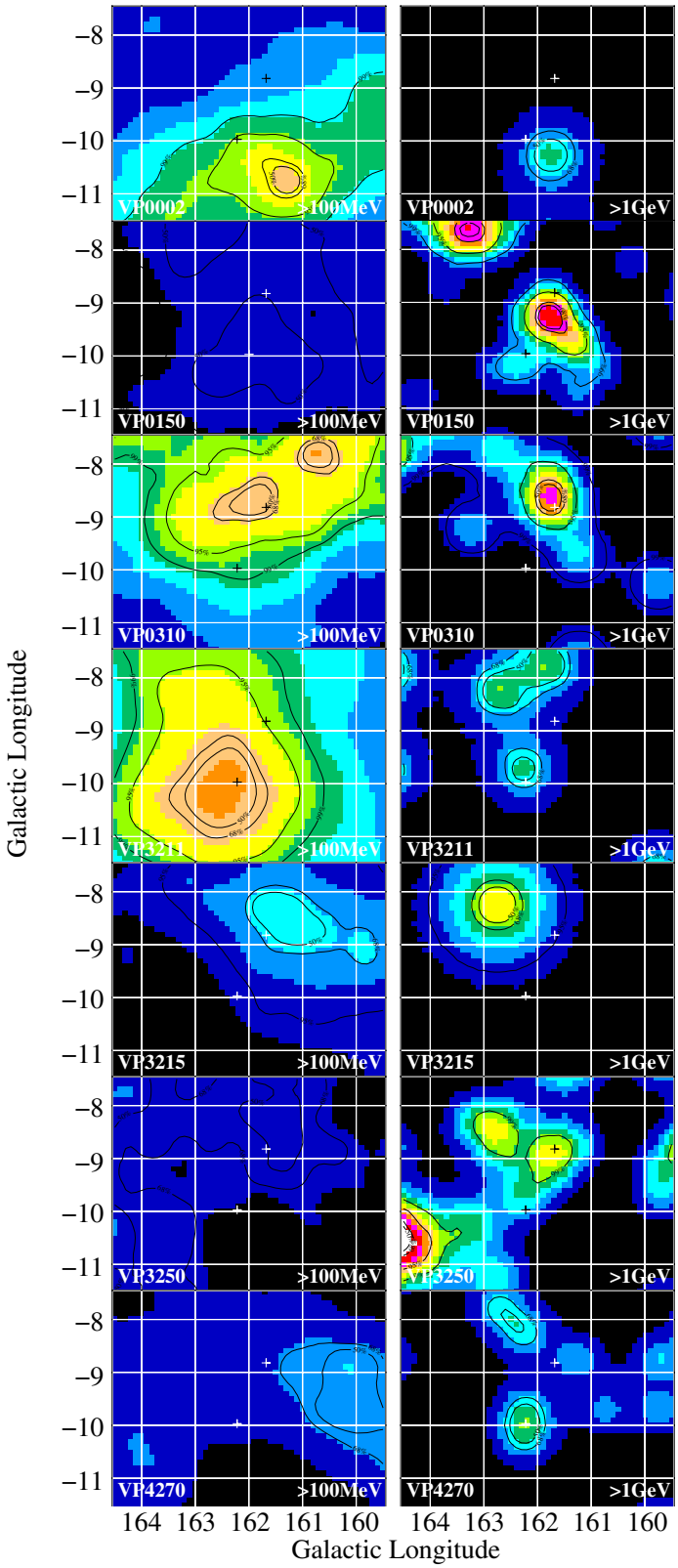

Fig. 1.— Likelihood maps for the seven viewing periods with TS>3 (anywhere in the map, either energy range). The left column panels are for E>100 MeV, while the right column panels show E>1000 MeV, with fewer photons but a considerably smaller point spread function. Crosses show the positions of 3C 111 and 3EG J0416+3650; ref. Figure 2.

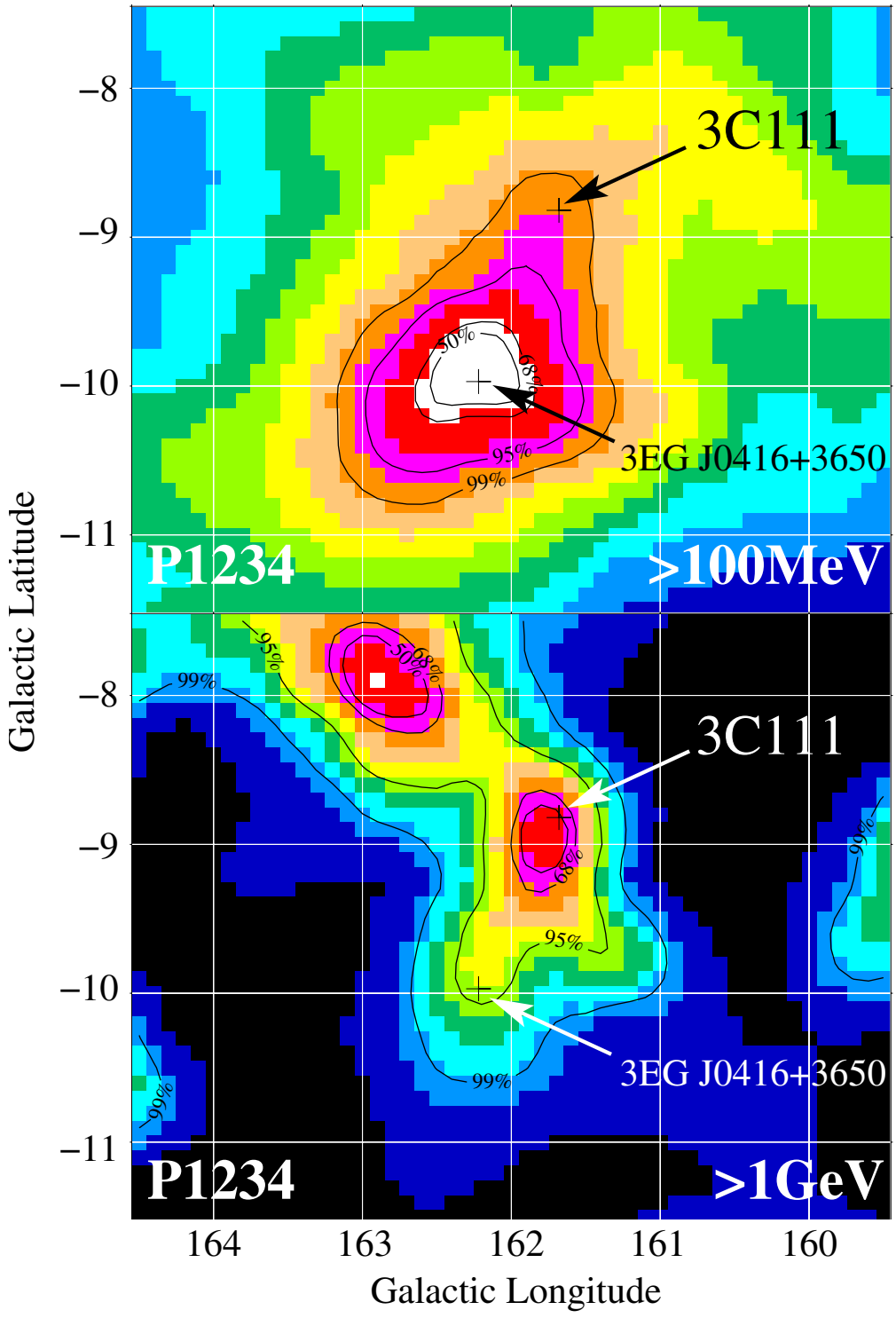

Fig. 2.— Likelihood maps for the summed exposure of all viewing periods, for >100 MeV (top) and >1000 MeV (bottom). On the scale used here, the position of Swift J041554.3+364926 is almost indistinguishable from that of 3EG J0416+3650, and is therefore not shown.

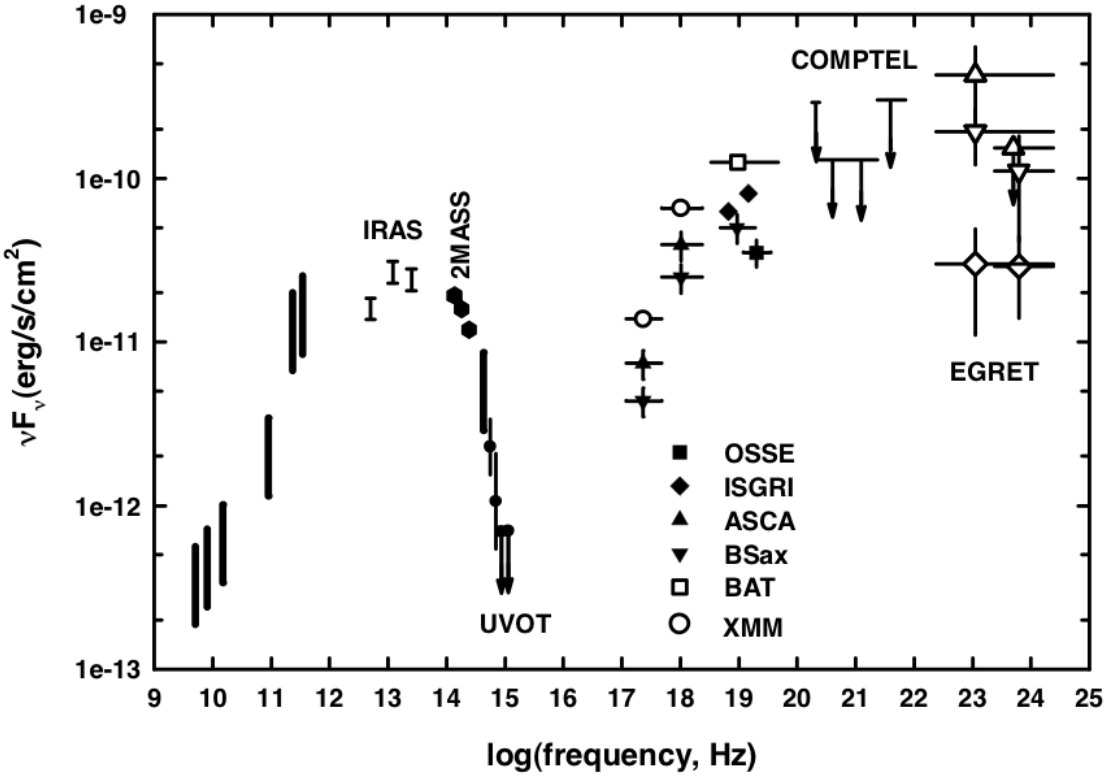

Fig. 3.— Spectral energy distribution for 3C 111. The data points are non-contemporaneous; their values and references are tabulated in Table 3. Thick vertical lines indicate historical ranges for radio and submillimeter observations. The thick vertical line in the optical indicates the range of R-band fluxes from 2004-2007 observations with the Liverpool Telescope - see text. The NIR through UV points have been dereddened; see text. For the EGRET data, the average values are indicated with open diamonds, the most significant single viewing period, VP0310, uses downward-pointing open triangles, and the maximum flux, VP3215, is shown with upward-pointing triangles. The lowest upper limits for a single VP (not shown) are similar to the average.

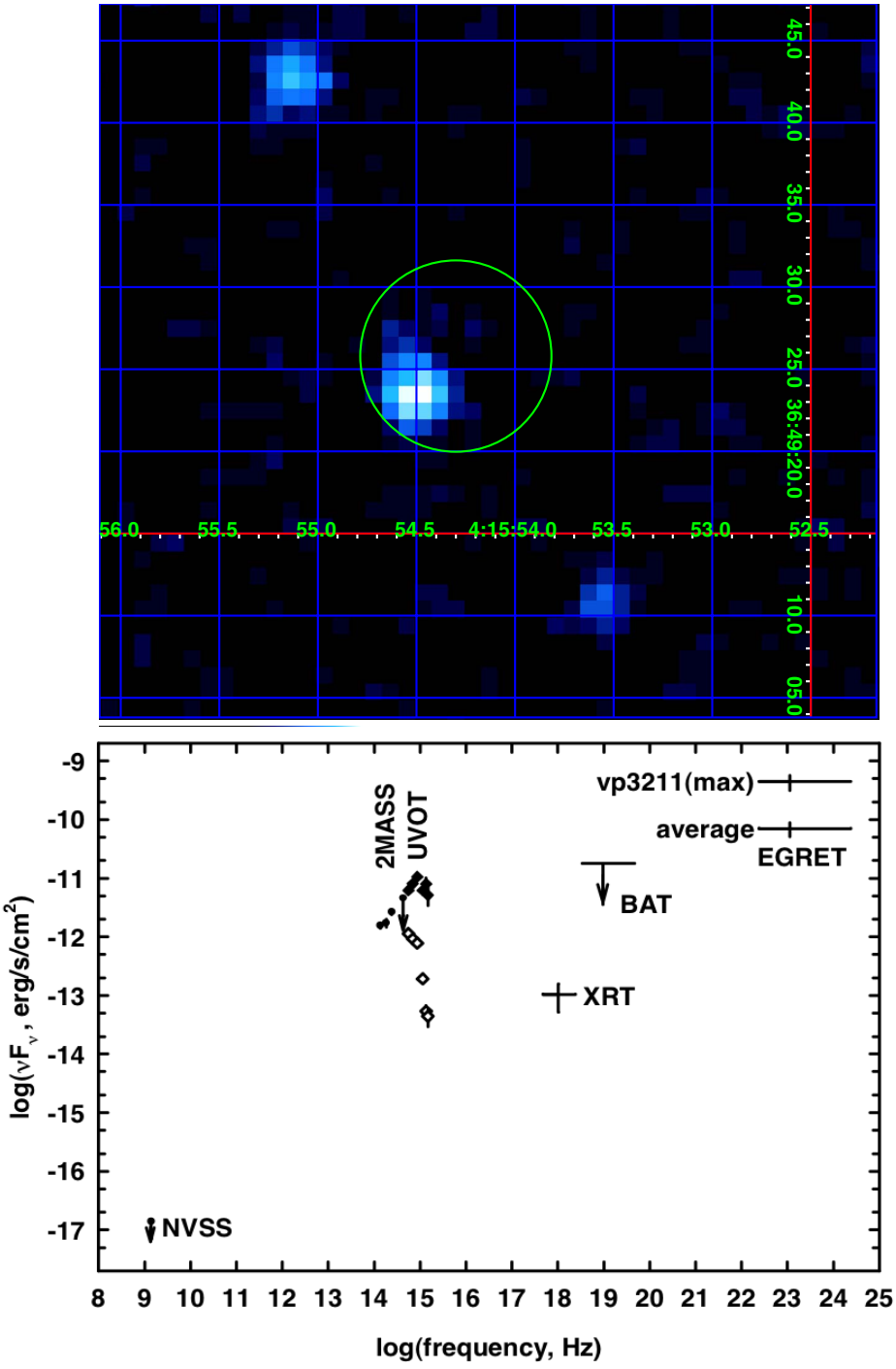

Fig. 4.— (a) UVOT image (UW1 filter) of the region around Swift J041554.3+364926. The circle indicates the position uncertainty (68% confidence) for the X–ray source; (b) Spectral energy distribution for Swift J041554.3+364926. The data points are non-contemporaneous; their values and references are tabulated in Table 3. For the UVOT data points, the observed values are shown as open circles, while dereddened values are shown as filled circles. The EGRET points may not be associated with the lower-frequency source - see text.

Table 1. EGRET detections of 3C 111 and 3EG J0416+3650 discussed in the main text.

				>100 MeV						>1000 MeV					
				3C 111			J J0416+3650			3C 111			J J0416+3650		
VP[a]	Start Date	Days	Off-Axis[b] [deg]	TS[c]	Offset[d] [deg]	Flux[e]	TS[f]	Offset[d] [deg]	Flux[e]	TS[c]	Offset[d] [deg]	Flux[e]	TS[f]	Offset[d] [deg]	Flux[e]
0002	04-22-1991	6	24.82		-	<33	18.3	1.2	60		-	<5	0.9	-	<11
0150	11-28-1991	14	10.01		-	<11	3.8	-	<19	10.8	0.43	2	0.8	-	<3
0310	06-11-1992	14	20.79	10.2	0.2	26	0.6	-	<25	8.9	0.19	3		-	<3
0390	09-01-1992	16	5.45		-	<13	1.6	-	<23	1.3	-	<4		-	<4
3211	02-08-1994	7	20.60		-	<33	17.1	0.2	55		-	<8	2.4	-	<11
3215	02-15-1994	2	20.60	9.0	0.5	64		-	<48		-	<20		-	<16
3250	04-26-1994	14	14.47	1.7	-	<24		-	<14	4.1	0.09	2	0.9	-	<5
4270	08-22-1995	16	7.91	3.0	-	<38	0.1	-	<22	0.2	-	<3	3.8	-	<4
P1234	–	–	—	2.7	-	<9	16.2	0.1	10	8.7	0.10	1	3.1	-	<1
9185	04-25-2000	14	25.65	0.1	-	<78		-	<75	0.3	-	<20		-	<8

[a]Only VPs with source detections are shown in this table. Seven additional VPs showed no indication of emission from either 3C 111 or 3EG J0416+3650 (see text). VP0390 (TS=0) is included here because it was the best exposure to the relevant sky region.

[b]Off-axis angle of 3C 111

[c]Maximum test statistic near the position of 3C 111

[d]Angle between the original position and the position of maximum TS

[e]Flux in units of 10^{-8} ph cm^{-2} s^{-1}

[f]Maximim test statistic near the position of 3EG J0416+3650

Table 2. >1000 MeV excesses $\geq 2\sigma$ in 17 maps (5° by 5°) of the field around 3EG J0416+3650.

VP	Full Field[a]	3C 111 Field[b]	0426+3747 Field[c]	Background Field[d]
0002	0	0	0	0
0005	s	0	s	0
0010	1	0	0	1
0150	2	1	1	0
0310	1	1	0	0
0360	1	0	0	1
0365	0	0	0	0
0390	1	0	0	1
2130	1	0	0	1
2210	1	0	1	1
3211	2	0	1	1
3215	s	0	s	0
3250	4	1	1	2
4120	2	0	0	2
4260	0	0	0	0
4270	1	0	0	1
8290	1	0	1	0
Sum	$18 + 2s$	3	$5 + 2s$	11
Rate	10%	18%	29%	7%

Note. — s (in VPs 0005, 3215, columns 2 and 4) - a single photon >1000 MeV very near the source position, probably significant because of the short exposures - see text; [a] 187 PSFs; [b] 17 PSFs; [c] 17 PSFs; [d] 153 PSFs

Table 3. 3C 111 SED data

Frequency[a]	Band	Instrument	Flux[b]	Flux Error	Reference[c]
$(0.24 - 24.1) \times 10^{23}$	$> 100\,\mathrm{MeV}$	EGRET(max)	1.92×10^{-10}	7.07×10^{-11}	(1)
$(2.41 - 24.1) \times 10^{23}$	$> 1000\,\mathrm{MeV}$	EGRET(max)	1.11×10^{-10}	7.00×10^{-11}	(1)
$(2.41 - 24.1) \times 10^{23}$	$> 1000\,\mathrm{MeV}$	EGRET(avge)	2.90×10^{-11}	1.50×10^{-11}	(1)
$(0.24 - 24.1) \times 10^{23}$	$> 100\,\mathrm{MeV}$	EGRET(avge)	3.00×10^{-11}	1.90×10^{-11}	(1)
$(0.24 - 24.1) \times 10^{23}$	$> 100\,\mathrm{MeV}$	EGRET(VP3215)	4.28×10^{-10}	2.06×10^{-10}	(1)
$(2.41 - 24.1) \times 10^{23}$	$> 1000\,\mathrm{MeV}$	EGRET(VP3215)	$< 1.53 \times 10^{-10}$		(1)
$(2.41 - 7.23) \times 10^{20}$	$1 - 3\,\mathrm{MeV}$	COMPTEL	$< 1.30 \times 10^{-10}$		(2)
$(7.23 - 24.1) \times 10^{20}$	$3 - 10\,\mathrm{MeV}$	COMPTEL	$< 1.30 \times 10^{-10}$		(2)
$(2.41 - 7.23) \times 10^{21}$	$10 - 30\,\mathrm{MeV}$	COMPTEL	$< 3.00 \times 10^{-10}$		(2)
$(1.81 - 2.41) \times 10^{20}$	$0.75 - 1\,\mathrm{MeV}$	COMPTEL	$< 2.90 \times 10^{-10}$		(2)
$(1.20 - 3.60) \times 10^{19}$	$50 - 150\,\mathrm{keV}$	OSSE	3.52×10^{-11}	6.56×10^{-12}	(3)
$(9.70 - 24.0) \times 10^{18}$	$40 - 100\,\mathrm{keV}$	ISGRI	8.10×10^{-11}	7.40×10^{-12}	(4)
$(4.80 - 9.70) \times 10^{18}$	$20 - 40\,\mathrm{keV}$	ISGRI	6.27×10^{-11}	5.70×10^{-12}	(4)
$(3.39 - 47.2) \times 10^{18}$	$14 - 195\,\mathrm{keV}$	BAT	1.25×10^{-10}	9.00×10^{-12}	(5)
$(4.80 - 19.3) \times 10^{18}$	$2 - 80\,\mathrm{keV}$	BeppoSax	4.99×10^{-11}	9.98×10^{-12}	(6)
$(4.80 - 24.0) \times 10^{17}$	$2 - 10\,\mathrm{keV}$	BeppoSax	2.49×10^{-11}	4.98×10^{-12}	(6)
$(1.20 - 4.80) \times 10^{17}$	$0.5 - 2\,\mathrm{keV}$	BeppoSax	4.36×10^{-12}	8.72×10^{-13}	(6)
$(4.80 - 24.0) \times 10^{17}$	$2 - 10\,\mathrm{keV}$	XMM	6.57×10^{-11}	3.94×10^{-13}	(6)
$(1.20 - 4.80) \times 10^{17}$	$0.5 - 2\,\mathrm{keV}$	XMM	1.38×10^{-11}	3.94×10^{-13}	(6)
$(4.80 - 24.0) \times 10^{17}$	$2 - 10\,\mathrm{keV}$	ASCA	3.92×10^{-11}	7.84×10^{-12}	(6)
$(1.20 - 4.80) \times 10^{17}$	$0.5 - 2\,\mathrm{keV}$	ASCA	7.42×10^{-12}	1.48×10^{-12}	(6)
1.14×10^{15}	UVW1	UVOT	$< 6.98 \times 10^{-13}$		(7)
8.57×10^{14}	U	UVOT	$< 6.95 \times 10^{-13}$		(7)
6.92×10^{14}	B	UVOT	1.00×10^{-12}	$(+1.0, -0.5) \times 10^{-12}$	(7)
5.55×10^{14}	V	UVOT	2.30×10^{-12}	$(+1.1, -0.7) \times 10^{-13}$	(7)
4.29×10^{14}	R	Liverpool	$(4.22 - 7.25) \times 10^{-12}$		(8)
2.40×10^{14}	J	2MASS	1.19×10^{-11}	4.00×10^{-13}	(9), (10)
1.82×10^{14}	H	2MASS	1.59×10^{-11}	4.62×10^{-13}	(9), (10)
1.36×10^{14}	K	2MASS	1.92×10^{-11}	3.66×10^{-13}	(9), (10)
2.50×10^{13}	12 micron	IRAS	2.43×10^{-11}	3.65×10^{-12}	(11)
1.20×10^{13}	25 micron	IRAS	2.69×10^{-11}	4.04×10^{-12}	(11)
5.00×10^{12}	60 micron	IRAS	1.61×10^{-11}	2.42×10^{-12}	(11)
3.40×10^{11}	0.85 mm	SMA	$(5.27 - 28.4) \times 10^{-12}$		(12)
2.30×10^{11}	1.3 mm	SMA	$(0.94 - 25.9) \times 10^{-12}$		(12)
9.00×10^{10}	3 mm	SMA	$(0.91 - 3.66) \times 10^{-12}$		(12)
1.50×10^{10}	2 cm	UMRAO	$(0.30 - 1.05) \times 10^{-12}$		(13)
8.00×10^{09}	3.6 cm	UMRAO	$(3.20 - 6.40) \times 10^{-13}$		(13)
5.00×10^{09}	6 cm	UMRAO	$(3.00 - 4.50) \times 10^{-13}$		(13)

[a]Frequency in units of Hz

[b]Flux in units of $\mathrm{erg\,cm^{-2}\,s^{-1}}$

[c]References: (1) this work; (2) Maisack et al. (1997); (3) Johnson et al. (1997); (4) Beckmann et al. (2006); (5) Tueller et al. (2007); (6) Kadler (2005); (7) F. Verrecchia, priv. comm.; (8) S. Jorstad, priv. comm.; (9) 2MASS archive; (10) Skrutskie et al. (2006); (11) Golombek et al. (1988); (12) SMA archive (`http://cfa-www.harvard.edu/rtdc/index-sma.html`); (13) Kadler et al. (2008)

Table 4. 3EG J0416+3650 SED data

Frequency[a]	Band	Instrument	Flux[b]	Flux Error	Reference[c]
$(0.24 - 24.1) \times 10^{23}$	$> 100\,\mathrm{MeV}$	EGRET(avge)	7.03×10^{-11}	1.89×10^{-11}	(1)
$(0.24 - 24.1) \times 10^{24}$	$> 100\,\mathrm{MeV}$	EGRET(VP3211)	4.42×10^{-10}	1.29×10^{-10}	(1)
$(3.39 - 47.2) \times 10^{18}$	$14 - 195\,\mathrm{keV}$	BAT	$< 1.78 \times 10^{-11}$		(2)
$(4.82 - 24.1) \times 10^{17}$	$2 - 10\,\mathrm{keV}$	XRT	1.05×10^{-13}	5.24×10^{-14}	(1)
1.48×10^{15}	UVW2	UVOT(observed)	4.43×10^{-14}	1.48×10^{-14}	(1)
1.34×10^{15}	UVM2	UVOT(observed)	5.38×10^{-14}	1.35×10^{-14}	(1)
1.14×10^{15}	UVW1	UVOT(observed)	1.94×10^{-13}	2.28×10^{-14}	(1)
8.57×10^{14}	U	UVOT(observed)	7.80×10^{-13}	3.43×10^{-14}	(1)
6.93×10^{14}	B	UVOT(observed)	9.29×10^{-13}	5.57×10^{-14}	(1)
5.55×10^{14}	V	UVOT(observed)	1.13×10^{-12}	9.40×10^{-14}	(1)
1.48×10^{15}	UVW2	UVOT(dereddened)	5.16×10^{-12}	1.72×10^{-12}	(1)
1.34×10^{15}	UVM2	UVOT(dereddened)	8.06×10^{-12}	2.02×10^{-12}	(1)
1.14×10^{15}	UVW1	UVOT(dereddened)	6.25×10^{-12}	7.38×10^{-13}	(1)
8.57×10^{14}	U	UVOT(dereddened)	1.06×10^{-11}	4.67×10^{-13}	(1)
6.93×10^{14}	B	UVOT(dereddened)	8.15×10^{-12}	4.89×10^{-13}	(1)
5.55×10^{14}	V	UVOT(dereddened)	6.22×10^{-12}	5.17×10^{-13}	(1)
4.29×10^{14}	R	2MASS	$< 4.58 \times 10^{-12}$		(3),(4)
2.40×10^{14}	J	2MASS	2.66×10^{-12}	2.66×10^{-13}	(3),(4)
1.82×10^{14}	H	2MASS	1.73×10^{-12}	2.60×10^{-13}	(3),(4)
1.36×10^{14}	K	2MASS	1.57×10^{-12}	1.57×10^{-13}	(3),(4)
1.40×10^{09}	20 cm	NVSS	$< 1.40 \times 10^{-17}$		(5)

[a]Frequency in units of Hz

[b]Flux in units of $\mathrm{erg\,cm^{-2}\,s^{-1}}$

[c]References: (1) this work; (2) Tueller et al. (2007); (3) 2MASS archive; (4) Skrutskie et al. (2006); (5) Condon et al. (1998)